Molecular Imaging
Volume 16 : 1-10
© The Author(s) 2017
Reprints and permission:
sagepub.com/journalsPermissions.nav
DOI: 10.1177/1536012117704768
journals.sagepub.com/home/mix
SAGE

Fluorescent, Plasmonic, and Radiotherapeutic Properties of the ^{177}Lu–Dendrimer-AuNP–Folate–Bombesin Nanoprobe Located Inside Cancer Cells

Héctor Mendoza-Nava, PhD[1,2], Guillermina Ferro-Flores, PhD[1], Flor de María Ramírez, PhD[3], Blanca Ocampo-García, PhD[1], Clara Santos-Cuevas, PhD[1], Erika Azorín-Vega, PhD[1], Nallely Jiménez-Mancilla, PhD[4], Myrna Luna-Gutiérrez, PhD[1], and Keila Isaac-Olivé, PhD[2]

Abstract

The integration of fluorescence and plasmonic properties into one molecule is of importance in developing multifunctional imaging and therapy nanoprobes. The aim of this research was to evaluate the fluorescent properties and the plasmonic–photothermal, therapeutic, and radiotherapeutic potential of ^{177}Lu–dendrimer conjugated to folate and bombesin with gold nanoparticles in the dendritic cavity (^{177}Lu–DenAuNP–folate–bombesin) when it is internalized in T47D breast cancer cells. The intense near-Infrared (NIR) fluorescence emitted at 825 nm from the conjugate inside cells corroborated the usefulness of DenAuNP–folate–bombesin for optical imaging. After laser irradiation, the presence of the nanosystem in cells caused a significant increase in the temperature of the medium (46.8°C, compared to 39.1°C without DenAuNP–folate–bombesin, $P < 0.05$), resulting in a significant decrease in cell viability (down to 16.51% $\pm$ 1.52%) due to the ^{177}Lu–DenAuNP–folate–bombesin plasmonic properties. After treatment with ^{177}Lu–DenAuNP–folate–bombesin, the T47D cell viability decreased 90% because of the radiation-absorbed dose (63.16 $\pm$ 4.20 Gy) delivered inside the cells. The ^{177}Lu–DenAuNP–folate–bombesin nanoprobe internalized in cancer cells exhibited properties suitable for optical imaging, plasmonic–photothermal therapy, and targeted radiotherapy.

Keywords

lutetium-177, radiolabeled dendrimers, radiolabeled nanoprobe, multifunctional radiopharmaceuticals, heterobivalent molecules, breast cancer, dendrimers, gold nanoparticles

Introduction

Different-sized gold nanoparticles (AuNPs) can be classified into molecular luminescent AuNPs (from 0.3 to 2 nm) and conventional plasmonic AuNPs (from 2 to 100 nm).[1] Luminescent AuNPs lack the characteristic surface plasmon resonance (SPR) due to the limited number of free electrons but can give a broad range of emissions from visible to near-Infrared (NIR) regions.[1] Due to their SPR, AuNPs can be used as localized heat sources for cancer treatment.[2,3] The photothermal conversion effect in AuNPs is based on the collective oscillations of the electrons under optical excitation, which provide strong localized heating when they are irradiated with a laser or exposed to a certain radiofrequency field.[3–5] The localized heating, reaching temperatures about of 700°C around AuNPs, causes irreversible thermal destruction of cancer tissues.[6–8]

[1] Departamento de Materiales Radiactivos, Instituto Nacional de Investigaciones Nucleares, Ocoyoacac, Estado de México, Mexico
[2] Facultad de Medicina, Universidad Autónoma del Estado de México, Toluca, Mexico
[3] Departamento de Química, Instituto Nacional de Investigaciones Nucleares, Ocoyoacac, Estado de México, Mexico
[4] CONACyT, Instituto Nacional de Investigaciones Nucleares, Ocoyoacac, Estado de México, Mexico

Submitted: 30/12/2016. Revised: 10/03/2017. Accepted: 21/03/2017.

Corresponding Author:
Guillermina Ferro-Flores, Departamento de Materiales Radiactivos, Instituto Nacional de Investigaciones Nucleares, Carretera México-Toluca S/N, La Marquesa, Ocoyoacac, Estado de México. C.P. 52750, México.
Emails: ferro_flores@yahoo.com.mx; guillermina.ferro@inin.gob.mx

The integration of fluorescence and plasmonic properties into one molecule is of importance in developing multifunctional imaging and therapy nanoprobes.[9,10]

Lutetium-177 is a β- and γ-emitting radionuclide with a physical half-life of 162 hours (6.73 days). In the field of nuclear medicine, an in vivo theranostic approach combines the potential of both diagnosis and therapy in the same targeting molecule by labeling with either a diagnostic (eg, ^{68}Ga) or a suitable therapeutic (eg, ^{177}Lu) radionuclide.[11,12]

Dendrimers are hyperbranched polymeric structures. Polyamidoamine (PAMAM) dendrimers are spherical macromolecules composed of repeating PAMAM units which are known to have high in vivo stability.[13,14] Unmodified cationic PAMAM dendrimers have been shown to be hemolytic, a property that was associated with their cationic nature. However, the construction of novel dendrimers with biocompatible components through the surface modification of commercially available dendrimers by PEGylation, acetylation, glycosylation, amino acid, vitamins, and peptide functionalization have solved the safety problem of dendrimer-based nanotherapeutics.[13]

Over the last 2 decades, several experimental evidences have suggested that the gastrin-releasing peptide (GRP) and other bombesin-like peptides act as growth factors in many types of cancer.[15] Overexpression of GRP receptors (GRPR) is present in 96% of breast cancer tissues.[16] The overexpression of folate receptor (FR)-α has been confirmed in all clinical breast cancer subtypes comprised of estrogen receptor (ER) positive, progesterone receptor (PR) positive, human epidermal growth factor receptor(HER2) positive, and triple negative (ER−, HER2−, PR−) tumors.[17–19] Therefore, heterobivalent conjugates of bombesin and folate are expected to improve the recognition of breast cancer cells positive to FR and GRPR.

The multifunctional theranostic radiopharmaceutical composed of AuNPs (size range: 1.0-2.9 nm) entrapped within the internal cavities of ^{177}Lu/^{68}Ga-labeled PAMAM and conjugated with target-specific molecules (bombesin and folate) at the periphery of the dendrimer has been recently synthesized as a potential optical and nuclear imaging agent for breast tumors as well as for targeted radiotherapy and plasmonic photothermal therapy.[20]

Nevertheless, fluorescent and plasmonic properties of radiopharmaceuticals based on AuNPs can significantly differ from those observed in vitro due to the possible AuNP aggregation inside cells.[21,22]

The aim of this research was to evaluate the fluorescent properties and the plasmonic, photothermal, therapeutic, and radiotherapeutic potential of the ^{177}Lu–DOTA–dendrimer–AuNP–folate–bombesin (^{177}Lu–DenAuNP–folate–bombesin) nanoprobe, when it is internalized in T47D breast cancer cells.

Experimental Methods

Preparation of ^{177}Lu–DenAuNP–Folate–Bombesin and DenAuNP–Folate–Bombesin

In this research, we used a ^{177}Lu–DenAuNP–folate–bombesin conjugate for which the carboxylate groups of bombesin and folic acid were covalently conjugated to the free amine groups of the dendrimer surface.[20] Elemental analysis, particle size distribution, transmission electron microscopy (TEM) analysis, ultraviolet (UV)-visible (Vis), scanning electron microscopy and X-ray analysis, infrared and fluorescence spectroscopies, and radio-HPLC analyses confirmed the dendrimer functionalization with high radiochemical purity (>95%).[20] Briefly, p-SCN-benzyl-DOTA (S-2-[4-Isothiocyanatobenzyl]-1,4,7,10-tetraazacyclododecane tetraacetic acid; 5.38 μmol, Macrocyclics, Dallas, Texas) was conjugated in aqueous–basic medium (bicarbonate buffer, 0.2 M, pH 9.5) to the G4-PAMAM-$(NH_2)_{64}$ dendrimer (0.3 μmol, Sigma-Aldrich Chemical Co, St Louis, Missouri). The carboxylate groups of Lys^{1}Lys^3(DOTA)-bombesin (0.55 μmol, piChem, Graz, Austria) and folic acid (2.27 μmol Sigma-Aldrich Chemical Co) were activated with HATU in DMF/DIPEA and also conjugated to the terminal amine groups of the PAMAM-G4 dendrimer. The conjugate was mixed with 1% $HAuCl_4$ followed by the addition of $NaBH_4$ and purified by ultrafiltration. A 15-μL aliquot (1.5 mg/mL) of the dendrimer–AuNP–folate–bombesin conjugate was diluted with 1 mol/L acetate buffer (35 μL, pH 5), followed by the addition of $^{177}LuCl_3$ (20 μL, 40 GBq/mL, >3 TBq/mg, ITG, Germany). The mixture was incubated at 90°C for 30 minutes. Radiochemical purity was >95% determined by size-exclusion radio-HPLC (ProteinPak 300SW, Waters, 1 mL/min, injectable grade water). This complex will be referred to as ^{177}Lu DenAuNP–folate–bombesin.

Since the radioactive material cannot be handled in TEM and fluorescent spectroscopy equipment, DenAuNP–folate–bombesin was used in these studies considering that few ^{177}Lu atoms (traces) are present in the ^{177}Lu DenAuNP–folate–bombesin system (MW ∼ 30 000 g/mol).

Cell Culture

The T47D breast cancer cell line was originally obtained from the American Type Culture Collection (Atlanta, Georgia). The cells were routinely cultured at 37°C with 5% CO_2 and 85% humidity in Roswell Park Memorial Institute medium (Sigma-Aldrich Co) supplemented with 10% fetal bovine serum and antibiotics (100 U/mL penicillin and 100 μg/mL streptomycin). These cells were selected since previously we have demonstrated an important uptake of ^{177}Lu–DenAuNP–folate–bombesin in T47D, which was significantly inhibited by preincubation with cold Lys^3-bombesin peptide or folic acid alone, indicating that the multifunctional system has specific recognition for GRPRs and FRs.[20]

Transmission Electron Microscopy

Transmission electron microscopy analyses were performed in order to corroborate the internalization of DenAuNP–folate–bombesin in T47D cells. Cells (5×10^5) were seeded into 6-well plates (Cyto-One, USA Scientific, Ocala, Florida) for 24 hours to allow adherence. DenAuNP–folate–bombesin was added to cells followed by 1 hour of incubation at 37°C. The

cells were washed 3 times with PBS, centrifuged into small pellets, and fixed with 2% glutaraldehyde and 2% paraformaldehyde in sodium cacodylate buffer (0.1 mol/L). The cells were further fixed with 1% osmium tetraoxide in 5 mmol/L 2-mercaptoethanol (phosphate–mercaptoethanol buffer), dehydrated in graded acetone series, and embedded in Epon-Spurr epoxy resin. Sections were cut at 85 nm using a diamond knife (Diatome, Hatfield Pennsylvania). The sections were stained with Sato's triple lead stain and 5% aqueous uranyl acetate for organelle visualization. The prepared samples were examined on a JEOL 1400 TEM microscope (JEOL, Peabody, Massachusetts) operating at 80 kV.

Fluorescence Imaging of DenAuNP–Folate–Bombesin Inside Cells

T47D cells (2×10^3) were grown on glass coverslips and following treatment with dendrimer (Den), Den-AuNP, and DenAuNP–folate–bombesin were rinsed with ice-cold PBS, fixed in acetone, and washed twice with PBS. After the addition of 250 μL (1 μg/mL) of Hoechst (DNA stain), cells were incubated for 1 minute at room temperature and rinsed with PBS before being mounted onto slides (ProLong Gold; Molecular Probes, Invitrogen Life Technologies, California). Hereinafter, the preparation of DenAuNP–folate–bombesin internalized in the T47D cells will be referred to as DenAuNP–folate–bombesin cell. Images of the fluorescent AuNPs of DenAuNP cell and DenAuNP–folate–bombesin cell were taken using an epifluorescent microscope (MeijiTechno MT6200; Saitama, Japan). Hoechst dye inside the nuclei was visualized with an excitation filter of 330 to 385 nm and using an emission filter of 420 nm. The AuNPs were detected using an excitation filter of 530 to 550 nm and an emission filter of 590 nm.

X-Ray Photoelectron Spectroscopy)

X-ray photoelectron spectra were acquired on a Thermo K-Alpha spectrometer equipped with an Al Kα X-ray source (1486.68 eV). The source was calibrated using Au $4f_{7/2}$ (84.0 eV) and Ag $3d_{5/2}$ (368.2 eV) from foil samples. An argon ion beam was used for charge compensation in the samples. The of DenAuNP–folate–bombesin and DenAuNP–folate–bombesin cell samples were introduced into an ultrahigh vacuum chamber of the spectrometer (1×10^{-7} to 1×10^{-8} Pascal) and measured at 297 K. The spot size in the beam was 200 μm. Twenty scans for Au4f were performed with an energy step size of 0.03 eV. Survey spectra were measured in the range of 0 to 1320 eV for DenAuNP–folate–bombesin (Supplemental Figure S1) and DenAuNP–folate–bombesin cell samples. The binding energies were referenced to the C1s peak at 285 eV. Shirley background subtraction was applied to all spectra. High-resolution spectrum was obtained for Au4f, C1s, and O1s bands. The Au4f spectrum was statistically analyzed using the Origin 8.1 software. The best fit was achieved for 4 peaks with a multipeak model and the Gaussian function with a correlation factor R^2 of .987 (DenAuNP–folate–bombesin), and for 6 peaks and the Lorentzian function with $R^2 = .994$ for the DenAuNP–folate–bombesin cell.

Fluorescence Spectroscopy Analysis of DenAuNP–Folate–Bombesin Inside Cells

Emission fluorescence spectra at 291 K of (1) DenAuNP–folate–bombesin cell sample, (2) T47D cells + Hoechst (matrix emission), and (3) T47D cell samples were recorded on a Perkin-Elmer LS-55 low-resolution luminescence spectrometer, from 200 to 900 nm (PerkinElmer, Inc., Santa Clara, California). All the samples were excited with wavelengths in the UV region to VIS region in order to distinguish between emission bands from the DenAuNP–folate–bombesin cell and those from the cells and remaining Hoechst dye themselves and to identify bands from Raleigh and Raman scatterings of the excitation lights used as well as harmonics bands in the VIS region from emission bands in the UV region (see Supplemental material). The best results for the 3 samples were obtained using excitation wavelengths (λ_{exc}) of 222, 270, 300, and 510 nm; emission filter of 290, 390, 430, and 515 nm, and excitation; and emission slits of 5 nm and 50 nm/min. To confirm some emission bands, excitation slit equals to 7 nm and emission slit equals to 10 nm were also tested. The source parameters were delay time (ms): 10, gate time (ms): 20, cycle time (ms): 33, and flash time: 3.

Phothothermal Plasmonic Potential of DenAuNP–Folate–Bombesin Inside Cells

T47D cells were incubated in a 96-well plate at a density of 5×10^3 cells/well. The cells were cultured for 24 hours at 37°C with 5% CO_2 and 85% humidity. Then, the culture medium was removed, the well plate was placed in a dry block heater at 37°C, and the cells were exposed to one of the following treatments (n = 6): (1) 100 μL of Den–folate–bombesin and 100 μL of PBS, pH 7 with irradiation (1.19 W/cm^2); (2) 100 μL of DenAuNP–folate–bombesin and 100 μL of PBS pH 7 with irradiation (1.19 W/cm^2); (3) 100 μL of distilled water (without nanoparticles) and 100 μL of PBS pH 7 with irradiation (1.19 W/cm^2); or (4) no treatment.

Laser irradiation in all experiments was conducted using a compact pulsed Nd: YAG laser (Q Smart 100; Quantel laser) pulsed for 5 ns at 532 nm (energy = 50 mJ/pulse) with a repetition rate of 10 Hz. The per-pulse laser power was measured using a Dual-Channel Joulemeter/Power Meter (Molectron EPM 2000; Coherent, Santa Clara, California). A diverging lens was used in the path of the laser beam such that the well plate was fully covered by the laser (diameter = 7 mm, area = 0.38 cm^2). The irradiance at the well plate was then calculated as the laser power per pulse divided by the laser spot area. Irradiation was performed for 6 minutes while delivering 1.19 W/cm^2 of average irradiance.

During laser irradiation, the temperature increase was measured using a type K thermocouple (model TPK-01) of immediate reaction that had been previously calibrated (probe diameter = 0.8 mm). The thermocouple was introduced into the well, and the temperature was registered each second using

a cold-junction-compensated K-thermocouple to digital converter (MAX6675, Maxim Integrated Products, Inc., San Jose, California) connected to a microcontroller board (Arduino Uno, Arduino AG Trademarks) with Universal Serial Bus (USB) computer connection. After irradiation, the solution of each well was removed and replaced with fresh medium.

The percentage of surviving cells in each well was evaluated by the spectrophotometric measurement of cell viability as a function of mitochondrial dehydrogenase activity, which involves the cleavage of the tetrazolium ring of sodium 3′-(1-[phenylaminocarbonyl]-3,4-tetrazolium)-bis(4-methoxy-6-nitro) benzene sulfonic acid hydrate (XTT) in viable cells to yield orange formazan crystals that are dissolved in acidified isopropanol (XTT kit, Roche Diagnostics GmbH, Mannheim, Germany). The resulting absorbance of the orange solution was measured at 480 nm in a microplate absorbance reader (Epoch, BioTek, Vermont). The absorbance of the untreated cells was considered as 100% of T47D cell viability.

Radiotherapeutic Potential: Cell Dosimetry

T47D cells were incubated in a 96-well plate at a density of 5×10^3 cells/well for 24 hours at 37°C with 5% CO_2 and 85% humidity. Then, the culture medium was removed, and the cells were exposed for 2 hours (at 37°C, with 5% CO_2 and 85% humidity) to one of the following treatments (n = 6): (1) 100 μL of $^{177}LuCl_3$ (74 kBq) and 100 μL of PBS, pH 7; (2) 100 μL of ^{177}Lu–DenAuNP (74 kBq) and 100 μL of PBS, pH 7; (3) 100 μL of ^{177}Lu–DenAuNP–folate–bombesin (74 kBq) and 100 μL of PBS, pH 7; or (4) no treatment.

After 2 hours, the solution in each well was removed and replaced with fresh culture medium. The cells were maintained for 3 days at 37°C with 5% CO_2 and 85% humidity. After that, the percentage of cell viability in each well was evaluated using the XTT kit method, as described earlier. The absorbance of the untreated cells was considered as 100% of T47D cell viability.

The calculation of absorbed dose in the cell was carried out by the Committee on Medical Internal Radiation Dose (MIRD) methodology using the cell internalization factors for ^{177}Lu–DenAuNP–folate–bombesine and ^{177}Lu–DenAuNP previously reported by Mendoza-Nava et al.[20] The internalized activity is considered the initial activity A_0. From the calculation of the total number of disintegrations during 3 days and the cell geometric factor (determined by Montecarlo using PENELOPE), the absorbed dose was computed.

Statistical Analysis

Comparisons between groups in laser irradiation and ^{177}Lu irradiation studies were made using the student *t* test (significance was defined as $P < 0.05$).

Results and Discussion

Transmission Electron Microscopy

Figure 1 shows that DenAuNP–folate–bombesin is internalized in T47D cells and exhibits vacuoles in the cell cytoplasm (Figure 1, top 3 panels) and on the cell membrane (Figure 1, bottom 2 panels). This specific recognition and internalization into the cell cytoplasm is attributed to the biological behavior conferred by bombesin and folate on the dendrimer surface which binds to GRPR and FR on the cell membrane.[20,23]

X-Ray Photoelectron Spectroscopy

The X-ray photoelectron spectroscopy (XPS) spectra of Au4f core orbitals of the DenAuNP–folate–bombesin system (Figure 2A) revealed 4 peaks corresponding to 2 doublets of the $4f_{7/2}$ and $Au4f_{5/2}$ orbitals of gold, which are shifted to larger binding energies with respect to those of the bulk gold metal (Au^0 atoms), 84.0 and 87.6 eV, (3.67 separation), respectively. The separation of the first doublets was 3.7 eV and the second one was of 3.8 eV. $Au4f_{7/2}$ peaks at 84.3 and 84.6 eV (shifted 0.3 and 0.6 eV) with Full-Width Half-Maximum (FWHM) = 0.8 eV, and $Au4f_{5/2}$ at 88.0 and 88.4 eV (shifted 0.4 and 0.8 eV) with FWHM = 1 eV, indicating that in the DenAuNP–folate–bombesin system, the encapsulated AuNPs are interacting with the amides and amines of the dendritic cavity with different degrees of strength because of the AuNP sizes that are between 2.1 and 2.9 nm[20] and the coexistence of Au^0 and any oxidized form. The treatment of the XPS spectrum and the extent of the shift suggest the presence of the AuNPs with the shorter diameter and/or the Au^{1+} oxidation state in the surface in about 20%. The shift of core Au4f electron peaks is inversely proportional to the grain size.[24] In AuNP-S-derivatives, where sulfur atoms are covalently bonded to AuNPs, the peak of Au^{1+} shifted significantly between 0.8 and 2.0 eV with respect to the Au^0 peak position. The coexistence of Au^0 and Au^{1+} atoms in the encapsulated AuNPs (diameter 2.5 ± 0.4 nm), and the stabilization that the conjugated dendrimer affords to the system, explain the particular fluorescence–plasmonic properties observed in the studied samples.

DenAuNP–folate–bombesin cell sample presented a particular XPS spectrum (Figure 2B). The positions of the peaks indicate the presence of 4 defined Au peaks centered at 82.3, 85.2, 89.6, and 94.2 eV, but the multipeak model using the Lorentzian function revealed 2 additional peaks on the left side (88.0 eV) and right side (90.6 eV) of the peak at 89.6 eV. The large shifts with respect to DenAuNP–folate–bombesin definitely point to a strong interaction of the conjugate system with the cells, which demonstrate that the conjugate was internalized in the cell, where it is not homogenously distributed and then exposed to different types of interaction with the cell. The $4f_{7/2}$ peak is located at 85.2 eV and $4f_{5/2}$ at 89.6 eV which has been associated with Au^{1+} with shifts of 0.9 and 1.6 eV with respect to the conjugate system before contact with the cell. This shift can also be due to the interaction of the encapsulated AuNPs with the amine and amide groups of cell proteins. However, the $4f_{5/2}$ peak is the most intense and broader than the $4f_{7/2}$ peak because of the contribution of the 2 peaks found by the fitting. This is an anomaly, since usually the $4f_{5/2}$ is less intense than the $4f_{7/2}$ peak. The band at 88.00 eV is associated with Au^0, but the other one seems to be an oxidized form of Au.

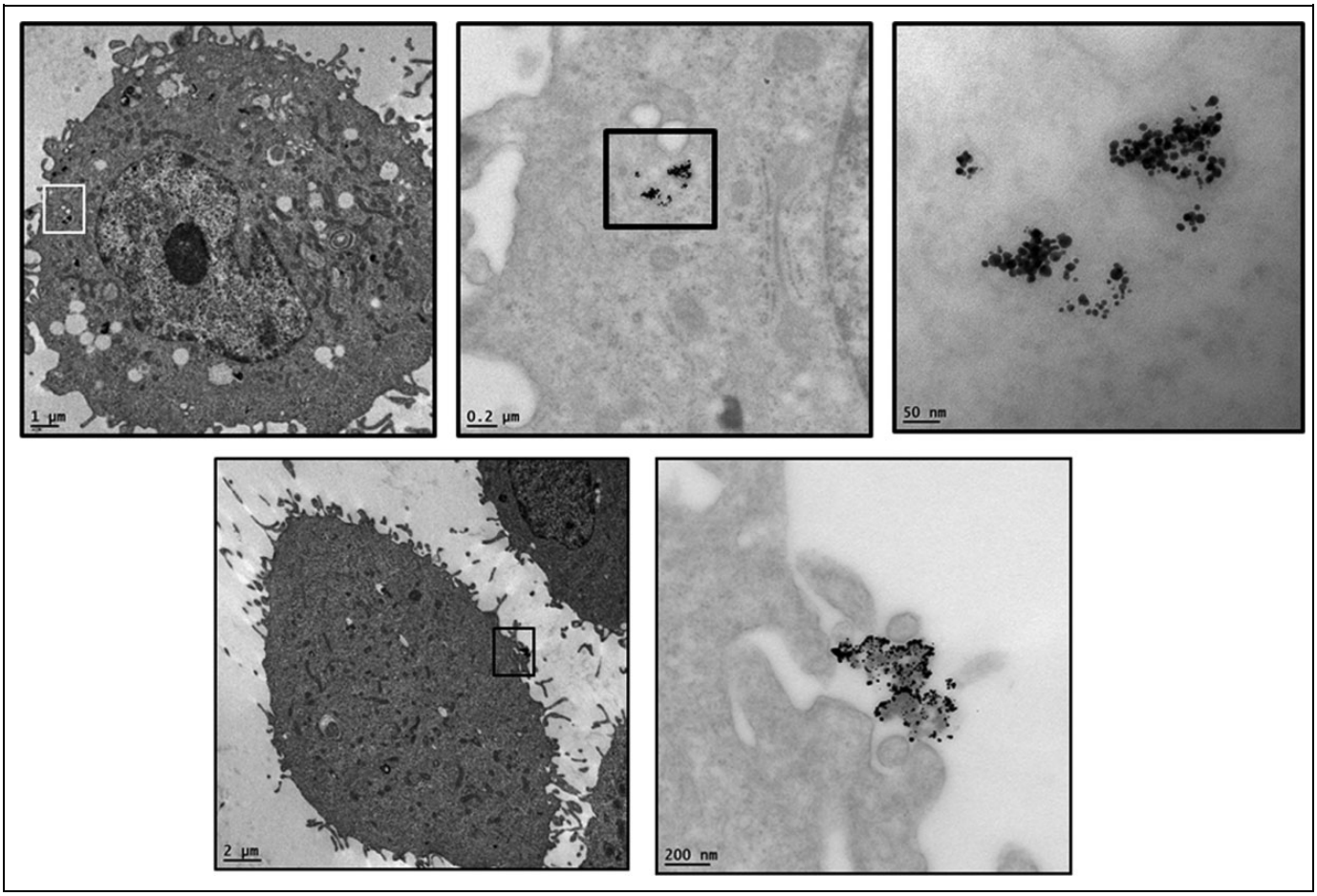

Figure 1. Transmission electron microscope (TEM) micrographs. Top panels: intracellular uptake in T47D breast tumor cells treated with DenAuNP–folate–bombesin for 2 hours. Bottom panels: DenAuNP–folate–bombesin in membrane showing a vacuole formation.

The band at 82.3 eV is too low in energy to correspond to Au^0 and that at 94.2 eV is too high for Au^{1+} oxidation states. This brings us to propose that once the DenAuNP–folate–bombesin is inside the cell, several interactions of the conjugate with anion and cation-transport cellular processes occur, which leads to chemical changes in the surface of the encapsulated AuNPs. Gold can have less common oxidation states such as -1, $+2$, and $+5$. Therefore, it would be possible that Au^0 atoms could be reduced to Au^{-1} atoms (auride anion), which is relatively stable due to the very high Pauling electronegativity of gold, and its ability to form salts with Ca, K, Cs, and Rb[25] and be oxidized to oxidation states higher than Au^{1+} ions (possibly 2+ and 3+ oxidation state). The presence of remaining Au^0 atoms and electrons from the Au^{1-} atoms on the surface of the encapsulated AuNPs (diameter 2.5 ± 0.4 nm) did not allow the plasmonic resonance band to extinguish in the DenAuNP–folate–bombesin cell sample.

Fluorescence Spectroscopy

The analysis of spectra recorded under different excitation wavelengths and emission filters allowed the discarding of emission bands from the cells and Hoechst dye, excitation light scatterings, and harmonic bands in the VIS-NIR region (which are broad usually) from the emission band in the UV region.

In Figure 3, the fluorescence emission spectrum of the DenAuNP–folate–bombesin cell (Figure 3A) is presented comparative to that of the DenAuNP–folate–bombesin conjugate (Figure 3B) obtained under the same experimental conditions. Regardless of the extent of the intensities, the intensity ratio of the UV/VIS-NIR bands of Figure 3A changed with respect to that of Figure 3B, and bands enveloped in the spectrum of the latter are revealed in the former. From 200 to 500 nm, the emission bands correspond to the organic components such as the functionalized dendrimer, the cells, and the Hoechst dye. Main bands in the VIS-NIR region (525-900 nm) of Figure 3B are clearly revealed in Figure 3A although slightly shifted. This points to the interaction of the DenAuNP–folate–bombesin with the cell. However, a sharp intense band at 825 nm is revealed. This lead to search of the origin of such a band. It was found that this band does not correspond to any scattered excitation light nor to first harmonic bands from the emission bands of the sample (for this test, the emission slit was larger than the excitation slit, Supplemental Figure S2), since it is present in the DenAuNP–folate–bombesin cell sample at the same position (± 2 nm) for all experimental conditions

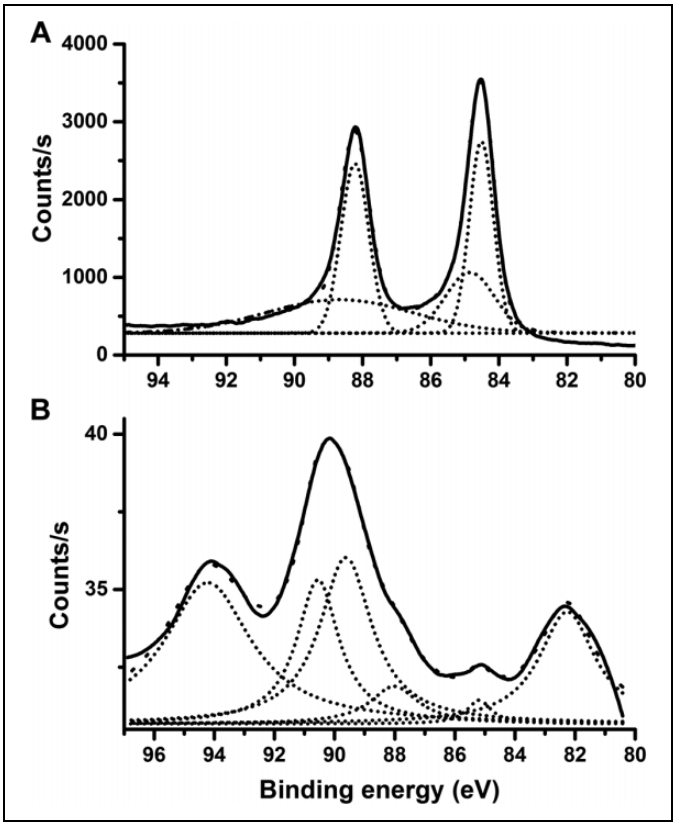

Figure 2. High-resolution X-ray photoelectron spectroscopy (XPS) spectra of the Au4f core orbitals of (A) DenAuNP–folate–bombesin and (B) DenAuNP–folate–bombesin cell.

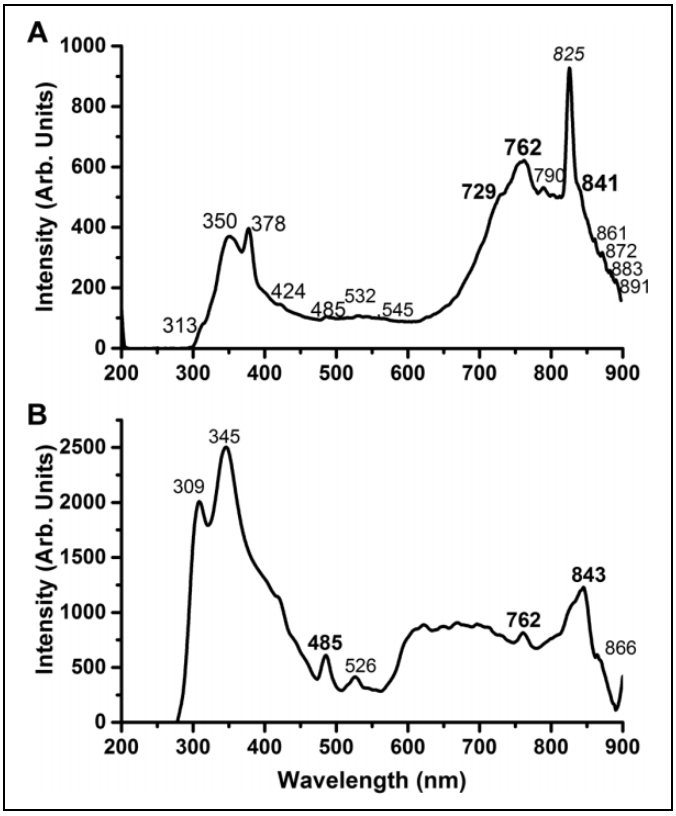

Figure 3. Fluorescence emission spectra of (A) DenAuNP–folate–bombesin cell, (B) DenAuNP–folate–bombesin. Excitation wavelength: 222 nm, filter 290 nm. Excitation and emission slits: 5 nm.

(Figure 3A and 4 and Supplemental Figure S2). It was seen as a poor band in the T47D cells and Hoechst dye spectra, and the relationship between them is probably that imines, imide, or imidazole groups are present in proteins and dyes such as Hoechst. The DenAuNP–folate–bombesin cell spectrum reveals more pronounced bands in the VIS (valence state effect) and NIR (surface ligand effect) regions than the DenAuNP–folate–bombesin, which indicates its internalization in T47D cells.

In Figure 4, the fluorescence emission spectra in the VIS-NIR region (525-900 nm) excited at 510 nm and with variable emission filters of (1) DenAuNP–folate–bombesin cell sample, (2) T47D cells + Hoechst, and (3) Hoechst are presented. The spectra from 200 to 900 nm are given in Supplemental Figures S3 and S4. In the spectra of the 3 samples (Figure S3 and S4), a shoulder at about 461 nm is observed, which corresponds to the fluorescence emission of the Hoechst dye. However, this emission is not the origin of the sharp band observed at 825 nm because the Stokes shift would be too large for any energy transfer and neither corresponds to a harmonic band, since these would appear beyond 900 nm. Figure 4 reveals an enhanced luminescence in the NIR region with a 515 nm emission filter, and the sharp band at 825 was the most intense at this condition. The emission filters did not diminish intensity in the (1) DenAuNP–folate–bombesin cell sample but disappeared in the (2) T47D cells + Hoechst sample, and it was negligible in the (3) Hoechst sample. The results demonstrated that DenAuNP–folate–bombesin was internalized in the cell and that the encapsulated stabilized AuNP of the DenAuNP–folate–bombesin system transfers its emission energy to a excited emission level already present in a component of the T47D cell proteins (receptors), where it is harvested and then reemitted with greater intensity. The emission bands from the DenAuNP–folate–bombesin system between 650 and 770 nm can act as an energy emission donor. However, in the T47D cells, the energy emission acceptor is the defined sharp band at 825 nm since being of low intensity became the most intense band excited at 510 nm with a 515-nm emission filter (Figure 4B) and excited at 222 nm with a 290-nm emission filter (Figure 3A). The enhanced emission fluorescence spectra of the DenAuNP–folate–bombesin cell sample under 2 extreme excitation light sources and those emission filters demonstrate that DenAuNP–folate–bombesin acts as a whole in the cells. The Stokes shifts between the bands in the 650 to 770 nm interval and that at 825 nm would be from 55 to 175 nm and point to a FRET mechanism in the energy transfer of DenAuNP–folate–bombesin to T47D cells (Förster resonance energy or fluorescence resonance energy transfer,[26–28] since the emission bands of DenAuNP–folate–bombesin are poorly shifted (1-3 nm) and the typical Förster distance for FRET (Ro = 1-100 nm) had to be fulfilled in DenAuNP–folate–bombesin cell.

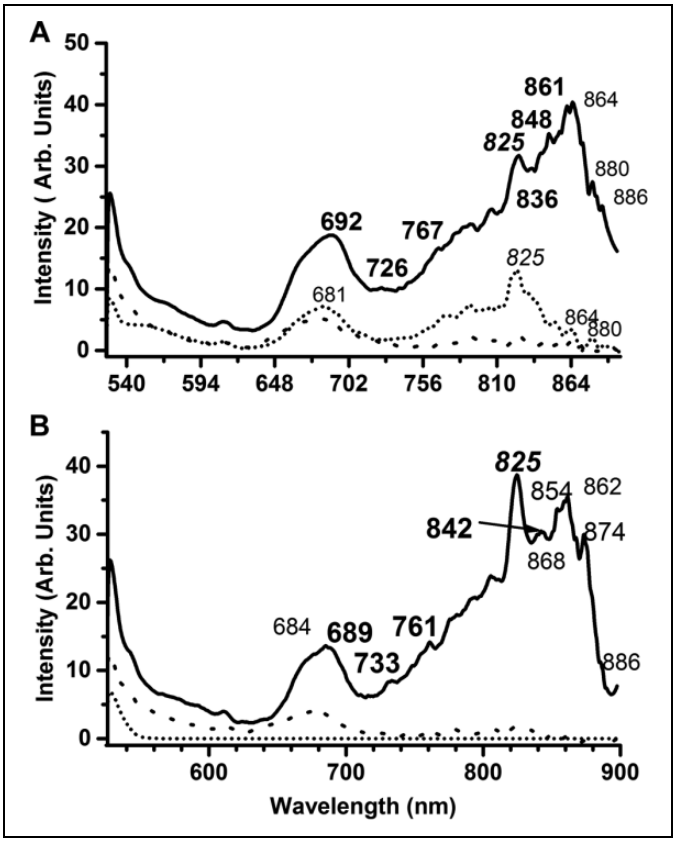

Figure 4. A, Fluorescence emission spectra in the visible (VIS)-near-Infrared (NIR) region of DenAuNP–folate–bombesin cell sample; Hoechst dye in cells (short dotted line) and Hoechst dye (dotted line). Excitation wavelength: 510 nm. Emission filter: 290 nm. B, Fluorescence emission spectra in the VIS-NIR region of DenAuNP–folate–bombesin cell sample. Hoechst dye in cells (short dotted line) and Hoechst dye (dotted line). Excitation wavelength: 510 nm. Emission filter: 515 nm.

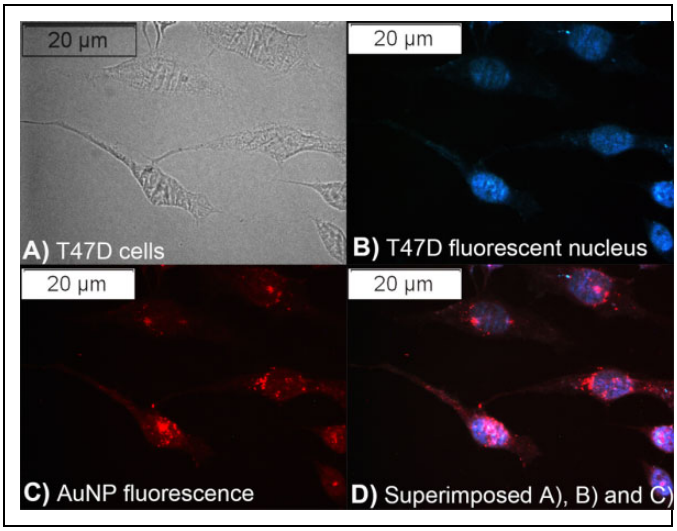

Figure 5. A representative microscopic field (×40) of T47D cells (A) in phase contrast, (B) the Hoechst stained nucleus, (C) the DenAuNP–folate–bombesin emission after 530 nm excitation, and (D) the merged nuclear and AuNP fluorescence images.

Small luminescent AuNPs (1.5-3.0 nm) can emit in the VIS region (valence state effect) and in the NIR region (surface ligand effect). This is the case of the DenAuNP–folate–bombesin, where the encapsulated AuNP has a diameter size between 2.1 and 2.9 nm.[20] The optical properties of the AuNPs are enhanced by their encapsulation in such a functionalized dendrimer because of the conformation and stabilization afforded by the macromolecule whose dendritic cavity interacts with AuNP through the tertiary amines and secondary amides. As a result of this interaction, about 16% of Au^0 atoms are oxidized to Au^{1+} atoms (see the X-Ray Photoelectron Spectroscopy section), and the resulting luminescence (fluorescence) is significant; the rest are Au^0 atoms (enough electron charge density), which is the main reason why the SPR band is still seen as a defined shoulder in the UV/VIS absorption spectrum but shifted to higher energy (approximately 510-515 nm) because of the small size of the AuNPs. It has been demonstrated that the SPR band of AuNP typically observed at 520 nm shifts to lower or higher energy in an inversely proportional mode to nanoparticle size.[29] In fact, it has been reported that an entrapped AuNP in a functionalized Dendrimer.G5 (Au-TOS-FA-DENPs) with AuNP size of 3.3 nm enhanced its luminescence and maintained its SPR at 520 nm.[30] Every day, new theoretical and experimental evidences appear, which demonstrate that AuNPs of diameters sizes between 1.5 and 4 nm are luminescent, that the SPR does not disappear, and that those with larger size where the SPR effect predominates also present luminescence. Although the fluorescence–plasmonic properties of AuNPs are dominated by the valence states of gold atoms and their particle sizes, it is clear from the above-mentioned evidence that the type and extent of their chemical environments can modify photophysical properties of AuNP systems significantly.

Fluorescence Imaging

Fluorescence images corroborate TEM results, demonstrating that DenAuNP–folate–bombesin is internalized in the cell. In this figure, the fluorescence of the nanoconjugate is seen as bright red dots that are localized either in the nuclei or in the cytoplasm of the cell.

The fluorescence spectra of DenAuNP–folate–bombesin cell sample (Figure 4) reveal emissions in the near-infrared region when it is excited at 510 and 222 nm. The emission bands between 650 and 850 nm regions are responsible for the visualization of the nanoparticles in the fluorescence imaging (Figure 5), under the recording conditions employed.

Effect of Laser Irradiation on Cell Viability

Figure 6 shows that the presence of AuNPs in the dendrimer significantly increased the temperature of the medium after laser irradiation (46.8°C, compared to 39.1°C without AuNPs within the dendrimer, $P < 0.05$). As expected, the increase in temperature of Den–folate–bombesin was similar to the control

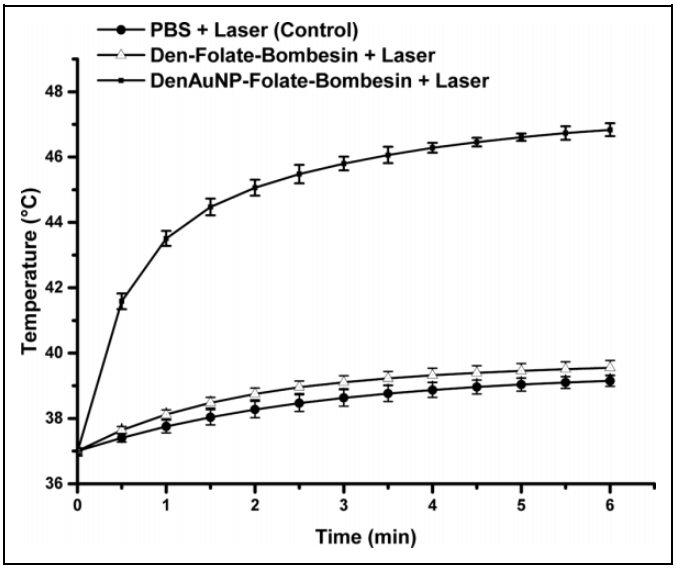

Figure 6. Medium temperature increase after laser irradiation of T47D cells incubated on the presence of Den–folate–bombesin, DenAuNP–folate–bombesin, and a control solution (irradiance: 1.1926 W/cm^2).

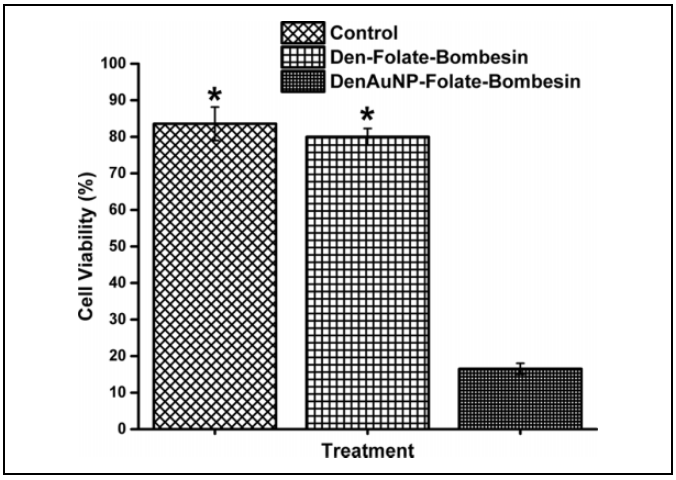

Figure 7. Effect on viability of T47D cells incubated on the presence of Den–folate–bombesin, DenAuNP–folate–bombesin, and the control after laser heating (irradiance 1.1926 W/cm^2). *Statistically significant difference ($P < 0.05$) versus DenAuNP–folate–bombesin.

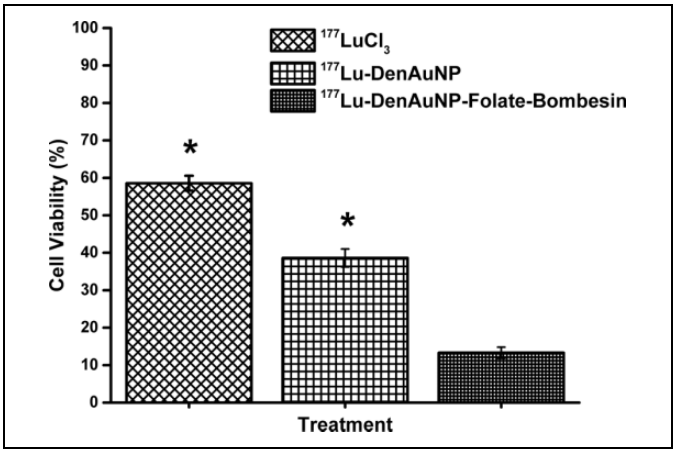

Figure 8. Effect of the radiation dose of $^{177}LuCl_3$, ^{177}Lu–DenAuNP, and ^{177}Lu–DenAuNP–folate–bombesin on T47D cell viability. *Statistically significant difference ($P < 0.05$) versus ^{177}Lu–DenAuNP–folate–bombesin.

sample (PBS), which indicates that changes in temperature are only determined by the presence of AuNPs within the dendrimer in the medium.

The effect of the temperature increase (plasmonic photothermal potential) in the studied treatments after laser irradiation is shown in Figure 6.

The DenAuNP–folate–bombesin system caused a significant decrease in cell viability ($P < 0.05$) down to 16.51% ± 1.52% by the end of treatment (6 minutes) when compared to Den–folate–bombesin (80.1% ± 2.28%; Figure 7). This result corroborated that the release of heat due to the nanoparticle (the expected temperature around each nanoparticle is 700°C) in the cytoplasm and the nucleus of T47D cells is the reason for the significant reduction in cell viability and not just the temperature increase in the medium during those few minutes.

Several trials have demonstrated a significant improvement in the clinical outcome when radiotherapy was conducted under hyperthermic conditions in patients. Hyperthermia increases the efficacy of radiotherapy by improving tumor oxygenation and interfering with the DNA repair mechanisms. However, the current techniques for hyperthermia induction display low spatial selectivity in the tissues heated. Lasers have been used to induce hyperthermia, and spatial selectivity can be improved by adding AuNPs within the dendrimer to the tissue to be treated. By exposing nanoparticles within the dendrimer to laser irradiation, it is possible to heat a localized area in the targeted cell without any harmful heating to the surrounding healthy tissues. The previous studies using AuNP for hyperthermia have demonstrated that the functionalization of AuNPs with probe molecules improves the particle accumulation in cell models significantly.[7,8] In this study, we have demonstrated that the system DenAuNP–folate–bombesin significantly reduces T47D breast cancer cell viability in comparison with Den–folate–bombesin after laser irradiation.

Radiotherapeutic Potential

As shown in Figure 8, the 3 studied treatments reduced the T47D cell viability, being significantly inhibited by ^{177}Lu–DenAuNP–folate–bombesin ($P < 0.05$). This effect is attributable to the greater T47D cell internalization of β-particles due to the folate and bombesin moiety. ^{177}Lu–DenAuNP does not affect cell viability as much as ^{177}Lu–DenAuNP–folate–bombesin but is higher than $^{177}LuCl_3$. ^{177}Lu–DenAuNP can be internalized in the cell by passive endocytosis, whereas $^{177}LuCl_3$ should not undergo cell internalization.

Table 1. Total Number of Disintegrations and Mean Absorbed Doses of ^{177}Lu Internalized in T47D Cancer Cells Within 3 Days (Monte Carlo simulation, PENELOPE 2008).

System	Source Region	Target Region	N = Total Disintegrations ($Bq * s$) Inside T47D Cells in 3 Days $\int_0^{t=3\ days} A(t)dt$	Absorbed Dose Per Disintegration ($Gy/Bq * s$)	Absorbed Dose, Gy
^{177}Lu^{177}Lu DenAuNP	Cell	Cell	323 295	$4.67 \times 10^{-5} \pm 3.11 \times 10^{-6}$	15.10 ± 1.01
^{177}Lu–DenAuNP–folate–bombesin			1 352 561		63.16 ± 4.20

The results of the cell viability (Figure 8) indicate that ^{177}Lu–DenAuNP–folate–bombesin is about 4 times more lethal than ^{177}Lu–DenAuNP. This experimental value is in accordance with the theoretical calculation of the absorbed dose shown in Table 1, where the absorbed dose of ^{177}Lu–DenAuNP–folate–bombesin is 4 times greater than that of ^{177}Lu–DenAuNP.

For absorbed dose calculation (Table 1), in each treatment, an activity of 14.8 Bq/cell (74 kBq/5000 cells) was used and the percentage of cell internalization of approximately 41% (6.07 Bq/cell) for ^{177}Lu–DenAuNP–folate–bombesin and 9.8% (1.45 Bq/cell) for ^{177}Lu–DenAuNP was considered as reported by Mendoza-Nava et al, with the consequent delivery of a therapeutic dose. The factor 4:1 obtained from the internalization fraction between ^{177}Lu–DenAuNP–folate–bombesin and ^{177}Lu–DenAuNP is in accordance with the lethality factor (4:1) and with the absorbed dose calculation (4:1).

Conclusion

The ^{177}Lu–DenAuNP–folate–bombesin nanosystem internalized in cancer cells exhibited properties suitable for optical imaging, plasmonic-photothermal therapy and targeted radiotherapy.

Declaration of Conflicting Interests

The author(s) declared no potential conflicts of interest with respect to the research, authorship, and/or publication of this article.

Funding

The author(s) disclosed receipt of the following financial support for the research, authorship, and/or publication of this article: This study was supported by the Mexican National Council of Science and Technology (CONACYT-SEP-CB-2014-01-242443). This research was carried out as part of the activities of the "Laboratorio Nacional de Investigación y Desarrollo de Radiofármacos, CONACyT". We thank Mr Rafael Basurto for his contribution with the XPS analysis. We thank the Electron Microscopy Core Facility Staff and Dr. K. Katti for the TEM images acquisition at the University of Missouri-Columbia.

Supplemental Material

The online supplemental figures are available at http://journals.sagepub.com/doi/suppl/10.1177/1536012117704768.

References

1. Zhou C, Yang S, Liu J, Yu M, Zheng J. Luminescent gold nanoparticles: a new class of nanoprobes for biomedical imaging. *Exp Biol Med (Maywood)*. 2013;238(11):1199–1209.
2. Fay BL, Melamed JR, Day ES. Nanoshell-mediated photothermal therapy can enhance chemotherapy in inflammatory breast cancer cells. *Int J Nanomedicine*. 2015;10:6931.
3. Wang L, Xu Y, Chen C. Near-infrared light-mediated gold nanoplatforms for cancer theranostics. In: *Advances in Nanotheranostics I*. Heidelberg, Germany: Springer Berlin; 2016:3–52.
4. Sanchez-Hernandez L, Ferro-Flores G, Jimenez-Mancilla NP, et al. Comparative effect between laser and radiofrequency heating of RGD-gold nanospheres on MCF7 cell viability. *J Nanosci Nanotechnol*. 2015;15(12):9840–9848.
5. Mendoza-Nava H, Ferro-Flores G, Ocampo-Garcia B, et al. Laser heating of gold nanospheres functionalized with octreotide: in vitro effect on HeLa cell viability. *Photomed Laser Surg*. 2013; 31(1):17–22.
6. Letfullin RR, Iversen CB, George TF. Modeling nanophotothermal therapy: kinetics of thermal ablation of healthy and cancerous cell organelles and gold nanoparticles. *Nanomedicine*. 2011;7(2): 137–145.
7. Luna-Gutierrez M, Ferro-Flores G, Ocampo-Garcia BE, et al. A therapeutic system of 177Lu-labeled gold nanoparticles-RGD internalized in breast cancer cells. *J Mex Chem Soc*. 2013; 57(3):212–219.
8. Jimenez-Mancilla N, Ferro-Flores G, Santos-Cuevas C, et al. Multifunctional targeted therapy system based on 99mTc/177Lu-labeled gold nanoparticles-Tat (49–57)-Lys3-bombesin internalized in nuclei of prostate cancer cells. *J Labelled Comp Radiopharm*. 2013;56(13):663–671.
9. Ferro-Flores G, Ocampo-Garcia BE, L Santos-Cuevas C, Morales-Avila E, Azorin-Vega E. Multifunctional radiolabeled nanoparticles for targeted therapy. *Curr Med Chem*. 2014;21(1): 124–138.
10. Cantelli A, Battistelli G, Guidetti G, Manzi J, di Giosia M, Montalti M. Luminescent gold nanoclusters as biocompatible probes for optical imaging and theranostics. *Dyes Pigm*. 2016;135(12): 64–79, doi:10.1016/j.dyepig.2016.06.019.
11. Ferro-Flores G, Ocampo-Garcia BE, Santos-Cuevas CL, de Maria Ramirez F, Azorin-Vega EP, Melendez-Alafort L. Theranostic radiopharmaceuticals based on gold nanoparticles labeled with

(177)Lu and conjugated to peptides. *Curr Radiopharm*. 2015; 8(2):150–159.
12. Banerjee S, Pillai M, Knapp F. Lutetium-177 therapeutic radiopharmaceuticals: linking chemistry, radiochemistry, and practical applications. *Chem Rev*. 2015;115(8):2934–2974.
13. Astruc D, Boisselier E, Ornelas C. Dendrimers designed for functions: from physical, photophysical, and supramolecular properties to applications in sensing, catalysis, molecular electronics, photonics, and nanomedicine. *Chem Rev*. 2010;110(4):1857–1959.
14. Orocio-Rodriguez E, Ferro-Flores G, Santos-Cuevas CL, et al. Two novel nanosized radiolabeled analogues of somatostatin for neuroendocrine tumor imaging. *J Nanosci Nanotechnol*. 2015; 15(6):4159–4169.
15. Sancho V, Di Florio A, Moody TW, Jensen RT. Bombesin receptor-mediated imaging and cytotoxicity: review and current status. *Curr Drug Deliv*. 2011;8(1):79–134.
16. Dalm SU, Martens JW, Sieuwerts AM, et al. In vitro and in vivo application of radiolabeled gastrin-releasing peptide receptor ligands in breast cancer. *J Nucl Med*. 2015;56(5):752–757.
17. Necela BM, Crozier JA, Andorfer CA, et al. Folate receptor-α (FOLR1) expression and function in triple negative tumors. *PLoS One*. 2015;10(3):e0122209.
18. O'Shannessy DJ, Somers EB, Maltzman J, Smale R, Fu YS. Folate receptor alpha (FRA) expression in breast cancer: identification of a new molecular subtype and association with triple negative disease. *Springerplus*. 2012;1(1):1–9.
19. Zhang Z, Li P, Chen H, et al. Folate receptor [alpha] associated with triple-negative breast cancer and poor prognosis. *Arch Pathol Lab Med*. 2014;138(7):890–895.
20. Mendoza-Nava H, Ferro-Flores G, Ramírez FdM, et al. 177Lu-dendrimer conjugated to folate and bombesin with gold nanoparticles in the dendritic cavity: a potential theranostic radiopharmaceutical. *J Nanomaterials*. 2016;2016(ID1039258):1–11, doi:10.1155/2016/1039258.
21. Goswami N, Yao Q, Luo Z, Li J, Chen T, Xie J. Luminescent metal nanoclusters with aggregation-induced emission. *J Phys Chem Lett*. 2016;7(6):962–975.
22. Wang SH, Lee CW, Pan MY, Hsieh SY, Tseng FG, Wei PK. Chromatogram analysis on revealing aggregated number and location of gold nanoparticles within living cells. *Plasmonics*. 2015;10(4):873–880.
23. Aranda-Lara L, Ferro-Flores G, Azorin-Vega E, et al. Synthesis and evaluation of Lys(alpha, gamma-folate)Lys(Lu-DOTA)-bombesin(1-14) as a potential theranostic radiopharmaceutical for breast cancer. *Appl Radiat Isot*. 2016;107:214–219.
24. Zheng J, Zhou C, Yu M, Liu J. Different sized luminescent gold nanoparticles. *Nanoscale*. 2012;4(14):4073–4083.
25. Jansen M. Effects of relativistic motion of electrons on the chemistry of gold and platinum. *Solid State Sci*. 2005;7(12): 1464–1474.
26. Surujpaul PP, Gutierrez-Wing C, Ocampo-García B, et al. Gold nanoparticles conjugated to [Tyr 3] octreotide peptide. *Biophys Chem*. 2008;138(3):83–90.
27. Oh E, Hong MY, Lee D, Nam SH, Yoon HC, Kim HS. Inhibition assay of biomolecules based on fluorescence resonance energy transfer (FRET) between quantum dots and gold nanoparticles. *J Am Chem Soc*. 2005;127(10):3270–3271.
28. Kraayenhof R, Visser AJ, Gerritsen H. Fluorescence spectroscopy, imaging and probes: new tools in chemical, physical and life sciences. Heidelberg, Germany: Springer Science & Business Media; 2012.
29. Huang X, El-Sayed MA. Gold nanoparticles: optical properties and implementations in cancer diagnosis and photothermal therapy. *J Adv Res*. 2010;1(1):13–28.
30. Zhu J, Zheng L, Wen S, et al. Targeted cancer theranostics using alpha-tocopheryl succinate-conjugated multifunctional dendrimer-entrapped gold nanoparticles. *Biomaterials*. 2014; 35(26):7635–7646.